

CrossHuman: Learning Cross-Guidance from Multi-Frame Images for Human Reconstruction

Liliang Chen*
OPPO Research Institute
Beijing, China

Han Huang[†]
OPPO Research Institute
Beijing, China

Jiaqi Li*
Beihang University
Beijing, China

Yandong Guo
OPPO Research Institute
Beijing, China

ABSTRACT

We propose CrossHuman, a novel method that learns cross-guidance from parametric human model and multi-frame RGB images to achieve high-quality 3D human reconstruction. To recover geometry details and texture even in invisible regions, we design a reconstruction pipeline combined with tracking-based methods and tracking-free methods. Given a monocular RGB sequence, we track the parametric human model in the whole sequence, the points (voxels) corresponding to the target frame are warped to reference frames by the parametric body motion. Guided by the geometry priors of the parametric body and spatially aligned features from RGB sequence, the robust implicit surface is fused. Moreover, a multi-frame transformer (MFT) and a self-supervised warp refinement module are integrated to the framework to relax the requirements of parametric body and help to deal with very loose cloth. Compared with previous works, our CrossHuman enables high-fidelity geometry details and texture in both visible and invisible regions and improves the accuracy of the human reconstruction even under estimated inaccurate parametric human models. The experiments demonstrate that our method achieves state-of-the-art (SOTA) performance.

KEYWORDS

Implicit Reconstruction, Multi-Frame Fusion, Transformer

1 INTRODUCTION

3D human reconstruction is a popular topic in computer vision and computer graphics, which is promising to enable various applications such as video games, holoportation and virtual try-on. To achieve surprisingly detailed geometry and texture reconstruction, existing methods [4, 12, 16, 27, 31, 36, 37, 50, 55, 57] often require multiple synchronized cameras, or a RGBD sensor. However, the expensive and professional setups limited their popularity. In contrast, single-view human reconstruction [5, 7, 20, 24, 35, 44, 45, 56] have enabled the recovery of 3D human pose and shape estimation using a single camera, which becomes a hot research topic due to its low cost and convenient setup.

Many single-view human 3D reconstruction methods have been proposed. Among which, tracking-based methods [3, 17, 18, 37, 53, 55, 61] utilize a statistical body template model as the geometrical prior and learn to deform the template, suffering from lack of fidelity



Figure 1: The results reconstructed using our method. Given only a RGB sequence, our method is able to reconstruct complete human with rich details even under very loose cloth.

and difficulty supporting clothing variations; while tracking-free methods [9, 10, 13, 22, 39, 44, 45] using implicit surface functions can handle topological changes and reconstruct the 3D human body with high-fidelity details in visible regions. However, these methods can not deal with challenging poses and the surfaces in the invisible regions are usually over-smooth.

In the recent work POSEFusion [28], the authors propose a human volumetric capture method that combines tracking-based methods and tracking-free inference methods to achieve dynamic and high-fidelity 3D reconstruction from a RGBD camera. They use the skeleton tracking to obtain the pose and shape parameters of SMPL [33] from depth stream, use pose-guided keyframe RGB image selection scheme to obtain more image details in visible and invisible regions, and finally fuse a complete human model. However, the RGBD camera is expensive and it is difficult for their method to deal with very loose cloth. In order to improve the accuracy of reconstruction system, the estimated parameters human model should be as accurate as possible. IP-Net [6] proposes a optimization based approach integrating viewpoint landmarks to optimize SMPL. PaMIR [60] designs a body reference optimization method to refine SMPL and uses the predicted SMPL at both the testing and the training stages. To a certain extent, such optimization methods can fill the accuracy gap of SMPL between different

*Both authors contributed equally to this research.

[†]Corresponding Author

stages, but the reconstruction quality is still strongly limited by the SMPL estimation.

State-of-the-art works of monocular SMPL estimation can output roughly correct pose and shape, but not very accurate. We believe that ordinary users' perception of the accuracy of reconstructing human body poses is relatively weak in many practical application scenarios. However, the slight SMPL pose estimation error will lead to many works that use SMPL priors to reconstruct the incomplete human body. The incomplete human reconstruction results are visually bad and will greatly affect the user experience. Therefore, we temporarily compromise on the insignificant pose error problem and try to find a way to both utilize the strong prior knowledge of SMPL model while avoiding the impact of SMPL error on reconstructed visual effects as much as possible. We hope to design a monocular reconstruction algorithm with practicality, integrity, realism, coherence and other elements of strong visual perception as primary goals.

To achieve high-quality geometry and texture reconstruction in both visible and invisible regions from a single RGB camera, in this paper we propose CrossHuman, which utilizes the estimated parametric human model and RGB images as guidance to reconstruct a complete human model. The geometry features of the SMPL serve as a coarse human shape proxy to guide our network handle challenging poses and encourage global shape regularity. Meanwhile, the pixel aligned features from multi-frame images lead to recover complex geometric and cloth wrinkles and resolve feature ambiguity. In addition, we further propose a new self-supervised training scheme in the CrossHuman-based framework, and achieve accurate reconstruction even under estimated inaccurate SMPL model. Our key contributions in this work can be summarized as follows:

a) A new single-view human 3d reconstruction pipeline that utilizes the parametric human model and RGB images as guidance, and achieves high-fidelity geometry and texture in both visible and invisible regions from a single RGB sequence.

b) The first method that relaxes the requirement of the SMPL accuracy. Our method achieves high-quality human 3D reconstruction in cases of inaccurate SMPL estimations and challenging poses.

c) A novel self-supervised training scheme that correct positions of warped points and a new transformer structure for multi-frame feature fusion. These modules effectively improve the reconstruction quality, contributing to deal with very loose cloth and wide body motion.

2 RELATED WORK

2.1 Implicit Representations

While explicit representations such as point cloud [1, 11, 29, 42], voxels [14, 32, 48, 51] and triangular meshes [5, 25, 26, 35, 38] have been explored to represent human 3D surface, these representations fail to represent high-quality 3D surfaces required for detailed human reconstruction.

Implicit 3D surface reconstruction methods [10, 19, 44, 45] defines a surface as a level set of a function of occupancy probability or surface distance. Recent works have shown promising results on human shape reconstruction based on deep implicit representations. PIFu[44] propose to regress a pixel-aligned implicit function and is able to reconstruct high-fidelity human surface based on

pixel-level image features. PIFuHD[45] extend PIFu for capture detailed reconstruction results with additional fine-level feature extraction network. Both methods lack the constrained priors of human body, which results in unstable performance especially for rare-seen poses.

2.2 Deep Implicit Reconstruction based on Human Priors

Previous works try to introduce human priors into deep implicit reconstruction. ARCH[21] and IP-Net[6] introduce SMPL model as parametric human representations. ARCH[21] proposed to regress 3D avatars in a canonical pose, but fails to generate accurate results, especially for loose clothes. IP-Net[6] jointly predict the 3D human model surface, the inner surface and body part labels from human point clouds. PAMIR[60] combines image features and SMPL volume features to reconstruct human surfaces, which can recover high-fidelity details in visible regions, but still over-smoothed in invisible areas in case of a single image setting. The SMPL volume feature helps PaMIR handle challenging poses, but when input SMPL is not accurate enough the reconstruction could be broken.

2.3 Tracking-based Human Reconstruction

Tracking-based methods [17, 18, 37, 53, 55, 61] utilize a pre-scanned human model as template and infer the deformation. DoubleFusion[55] propose a real-time human 3D reconstruction system that combines volumetric reconstruction with parametric human model from a single depth camera. However, this method cannot effectively give the dynamic 3D reconstruction results of human body wearing very loose cloth and cannot effectively deal with the geometrical topological changes of human body. POSEFusion[28] leverages tracking-based and tracking-free methods to achieve high-fidelity human surfaces using a RGBD camera. It fuses the features extracted from keyframe, and obtain the information of the invisible area of the human body. However, POSEFusion cannot deal with very loose cloth and the hardware costs limit its popularity.

3 METHOD

An overview of our approach is illustrated in Fig. 2, the cross guidance learned from RGB sequence and parametric body contribute to the high-fidelity reconstruction.

We obtain the SMPL model from the whole RGB sequence, and select reference frames for each target frames (Section 3.1). In the training stage, we sample points near the 3D ground truth with similar strategies presented in PIFu. In the testing stage, we allocate a volume space and create a grid by resolution. We bind the points (voxels) to the SMPL vertices (Section 3.2) and warp the points (voxels) to reference frame spaces (Fig. 3), so that we can fuse features from different frames(Section 3.3). Fused features are used to predict occupancy or color (Section 3.5) through Multilayer Perceptron (MLP). The mesh can be extracted using Marching Cubes [34]. However, warped points (voxels) are not necessarily close to the true human body surface when people wear loose cloth or the SMPL model is inaccurate. To this end, we propose a self-supervised training scheme for warp refinement (Section 3.4), which could correct the wrong warping and bring the warped point closer to the true human body surface.

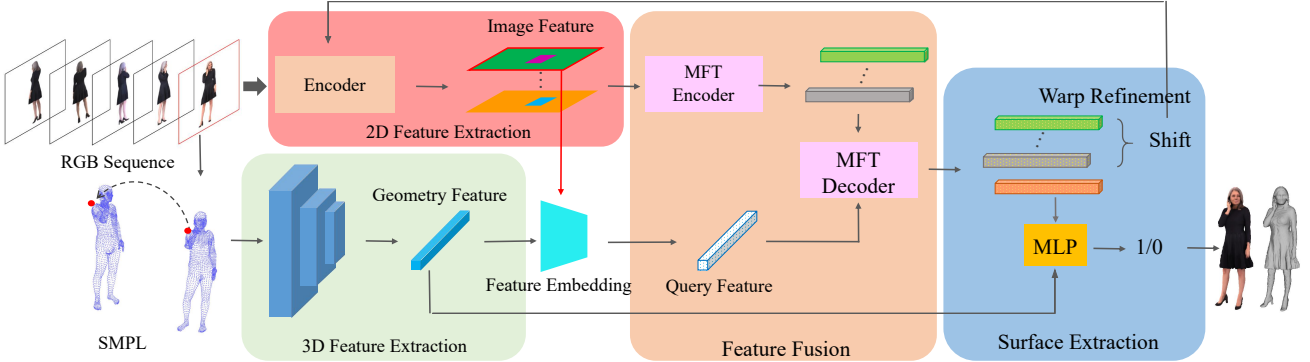


Figure 2: Overview of our CrossHuman pipeline. The framework consists of five components: i) reference frames selection, SMPL-guided tracking and warping ii) image feature and SMPL geometry feature extraction iii) multi-frame feature fusion, iv) warp refinement v) occupancy or color inference.

3.1 Reference Frames Selection

From the whole RGB sequence, the current i -th frame is described as target frame in this paper. Inspired by POSEFusion [28], we use pose-guided frame selection to choose reference frames. The key points for selecting reference frames are the complementarity of visible areas and the similarity of poses from other frames. We track the SMPL model from the whole RGB sequence, and select N ($N = 4$ in our experiments) reference frames.

According to the visibility complementarity, we can select reference frames from different angles of the human body to get a complete surface information about the human body. Pose similarity is defined as the similarity between the reference frame pose and the target frame pose. Based on pose similarity of the SMPL model, we calculate the pose-guided frame selection function between target frame and j -th reference frame as:

$$F_{pose}(i, j) = \sum_{k \in \mathcal{J}} \omega_k \left| \theta_i^k - \theta_j^k \right|^2 + \frac{\omega_{k'}}{\left| \theta_i^{k'} - \theta_j^{k'} \right|^2} \quad (1)$$

where \mathcal{J} is the joint index set of the SMPL model except the global rotation and translation, k' is the global rotation and translation, and the ω_k is the weight of the k -th joint to the reference frame, θ denotes the rotation angle for the joint. In this work, the whole pipeline is assumed to be off-line, so we can precompute reference frames for each frame in a video sequence before running reconstruction frame by frame.

3.2 SMPL-guided Tracking

Parametric body Model Inspired by POSEFusion and PaMIR, we integrate the parametric SMPL model to guide the warp of space and regularize the human reconstruction. SMPL is a skinned model with 6890 vertices, and it is defined as a function of shape parameters and pose parameters. The function $M(\theta, \beta)$ is formulated as:

$$\begin{aligned} M(\theta, \beta) &= W(T(\theta, \beta), J(\beta), \theta, \mathcal{W}) \\ T(\beta, \theta) &= \bar{T} + B_s(\beta) + B_p(\theta) \end{aligned} \quad (2)$$

where $W(\cdot)$ is a linear blend-skinning function with deformed body shape $T(\cdot)$, pose parameters θ , skeleton joints $J(\beta)$ and skinning weights \mathcal{W} , which returns the posed vertices. The deformed SMPL model can also serve as a geometry prior, which regularize the human reconstruction.

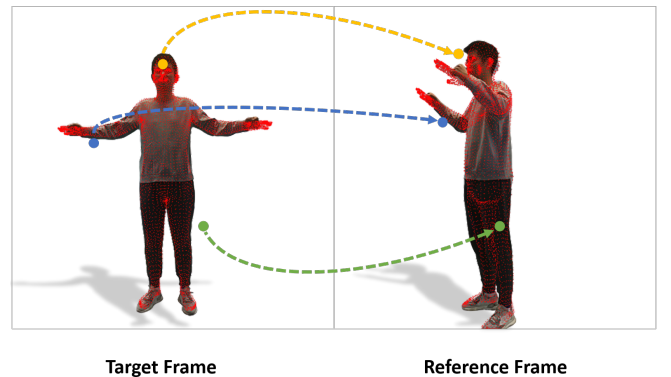


Figure 3: Points Warping. Points bound to the SMPL model are warped to reference frame spaces to fetch corresponding features through body motion tracking.

Sampling, Binding and Warping To ensure the temporal continuity, we use video based SMPL estimation method [24] to track the SMPL model from the whole sequence. The SMPL estimation module used in our framework can be replaced by any other SMPL estimation algorithm for monocular video. According to PIFu [44], the sampling strategy can affect the quality of reconstruction. In the training stage, we first randomly sample points on ground truth body surface in the target frame space and add offsets with normal distribution $N(0, \sigma)$ ($\sigma = 0.05$ cm in our experiments) for x , y , and z axis. We then uniformly sample points within a 3D bounding box containing the ground truth body. Finally, We mix uniformly

samples points and points nearby the surface. In the testing stage, we allocate a volume space and create a grid by resolution. After sampling, we bind the points (voxels) to SMPL vertices and warp the points (voxels) to reference frame space by SMPL motion (Fig. 3). The warp matrix $M_i(\theta, \beta)$ of v_i from T-pose to the other pose is computed by:

$$M_i(\theta, \beta) = \left(\sum_{j=1}^K W_{i,j} G_j \right) \begin{bmatrix} \mathbf{I} & B_{S,i}(\beta) + B_{P,i}(\theta) \\ 0^T & 1 \end{bmatrix} \quad (3)$$

where the blend weight $W_{i,j}$ is defined as the influence of rotation of part j on the vertex v_i , G_j is the world transformation of joint j , $B_{S,i}(\beta)$ is pose blendshape, and $B_{P,i}(\theta)$ is shape blendshape.

we define the warp of SMPL vertices from one pose x_1 to another pose x_2 in the SMPL coordinate system as:

$$\begin{bmatrix} x_2 \\ 1 \end{bmatrix} = M_i(\beta, \theta_2) M_i^{-1}(\beta, \theta_1) \begin{bmatrix} x_1 \\ 1 \end{bmatrix} \quad (4)$$

We found that binding strategies influence the accuracy of warp. Consider the fact that a sampled point might be bound to different body parts, leading to non-meaningful or even wrong warp. In order to improve the accuracy of warp, we bind each sampled point to the three SMPL vertices closest to it, and divide the SMPL vertices into 14 parts, including hand, head and torso, etc. If the SMPL vertices bound to one sampled point belong to the same part or neighboring parts, the warp matrix of the three SMPL vertices will be weighted. If the bound SMPL points belong to the non-neighboring parts, the sampled point will be ignored (Fig. 4). The warp weight is designed as:

$$\omega_{j \rightarrow i} = \exp\left(\frac{\|p_j - v_i\|}{2\sigma^2}\right) \quad (5)$$

$$\omega_i = \sum_{j \in \mathcal{N}(i)} \omega_{j \rightarrow i}$$

Where p_j is a 3D sampled point, v_i is a SMPL vertex, $\mathcal{N}(i)$ is the SMPL vertex closest to the p_j and $\mathcal{N}(i) = 3$, $\omega_{j \rightarrow i}$ is the binding weight, and ω_i is the weight normalizer.

We can warp the sampled points from one pose to another pose as:

$$\begin{bmatrix} p_2 \\ 1 \end{bmatrix} = \sum_{j \in \mathcal{N}(i)} \frac{\omega_{j \rightarrow i}}{\omega_i} M_i(\beta, \theta_2) M_i^{-1}(\beta, \theta_1) \begin{bmatrix} p_1 \\ 1 \end{bmatrix} \quad (6)$$

Due to the limitation of the SMPL parametric model, the estimated hands and feet of the SMPL body are usually not accurate, which affects the warp of the hand and foot. In this work, we shielded the hands and feet from binding (Fig. 4).

3.3 Feature Fusion

Thanks to the SMPL-guided tracking, one can achieve spatially aligned local features by projecting warped points to multi-frame feature maps. Straight-forward ways to fuse those features from different frames are operations like average pooling [44] or self-attention [59]. To force SMPL geometry and multi-frame RGB jointly guide the feature fusion, we design a multi-frame transformer (MFT). The MFT adopts self-attention based encoder-decoder architecture inspired by view-to-view transformer proposed in DoubleField [46].

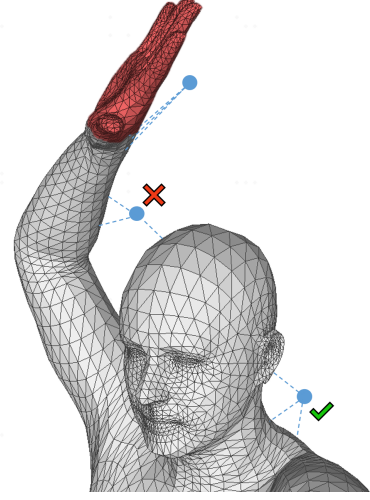


Figure 4: Points Binding

The MFT encoder fuse features from multi-frame images with self-attention operation in Eq[7]:

$$\begin{aligned} \varphi^i &= \varphi(x, I_i) \\ Q^e, K^e, V^e &= F_{Q,K,V}^e(\varphi^1, \varphi^2, \dots, \varphi^n) \\ \Phi &= F^e(\text{Att}(Q^e, K^e, V^e)) \end{aligned} \quad (7)$$

where φ^i is pixel-aligned feature of points x on image I_i . $F_{Q,K,V}^e(\cdot)$ denotes the linear layers, which output the query, key and value matrices, $\text{Att}(\cdot)$ is the multi-head attention operation, F^e is the feed-forward layer.

A feature embedding combined with target frame image feature and SMPL geometry feature works as the query feature in MFT decoder. The decoder enables the cross-attention between the query feature and multi-frame features. To be more specific, the operation can be formulated as:

$$\begin{aligned} \phi_q &= E_q(\oplus(\varphi(x, I_t), \Psi(x, S_t))) \\ \phi_Q, \phi_K, \phi_V &= F_{Q,K,V}(\Phi, \phi_q) \\ e_o, e_s &= F^e(\text{att}(\phi_Q, \phi_K, \phi_V)) \end{aligned} \quad (8)$$

where $\Psi(\cdot)$ is a function extracting SMPL geometry feature. S_t is the SMPL parameters for target frame, \oplus is a concatenate operator, E_q is used to generate query feature embedding, $F_{Q,K,V}$ is the linear layers, $\text{att}(\cdot)$ is the attention operation in the transformer, and F^e is the feed-forward layer.

The MFT decoder outputs a fused feature embedding e_o and a multi-frame feature block e_s . The fused feature embedding is used for occupancy and texture inference through MLP g and the multi-frame feature block is fed to another MLP s for predicting warp refinement.

$$g(\oplus(e_o, \Psi(x, S_t))) = \text{Occupancy} \quad (9)$$

$$s(e_s) = \text{Noise} \quad (10)$$

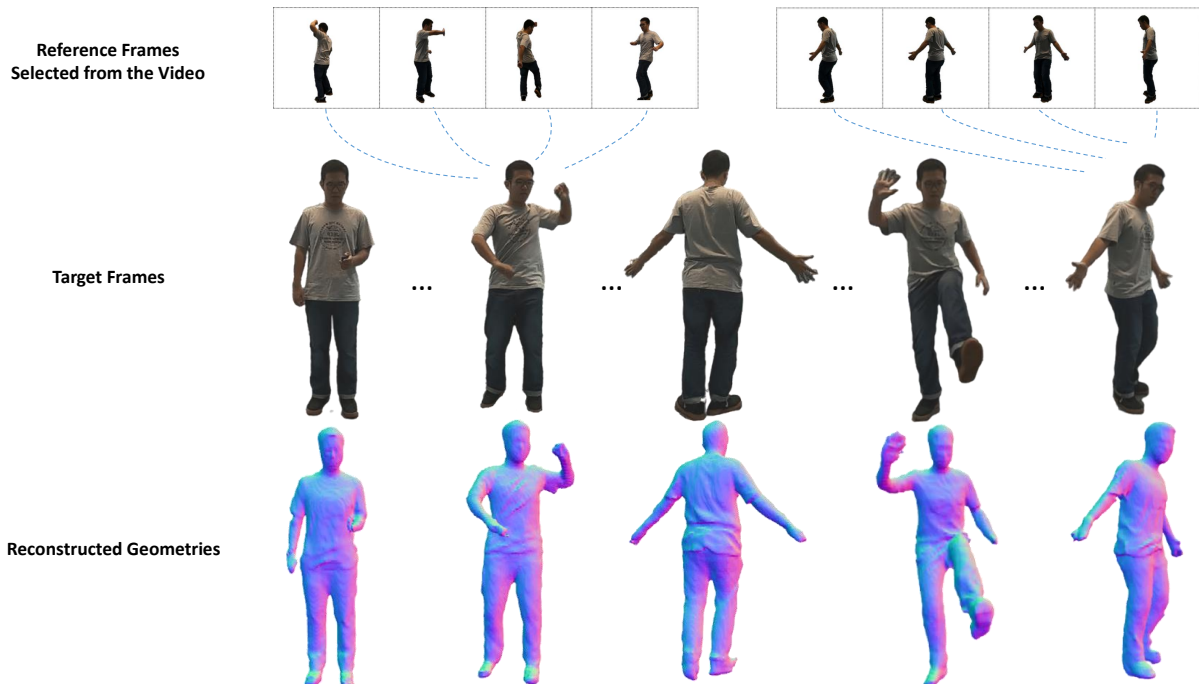


Figure 5: Dynamic Results on Real Video

3.4 Warp Refinement

For the network that utilizes parametric human model to reconstruct human body, the accuracy of the parametric human model greatly affects the accuracy of the reconstruction system. In this work, we propose a self-supervised training scheme, which could improve the accuracy of the reconstruction system in the cases of estimated inaccurate SMPL model and very loose cloth. In training stage, we randomly add noise shift to warped 3D points and feed the multi-frame feature block output by MFT to an MLP for predicting the random noise shift. We adopt iterative error feed back strategy [23, 58] for progressive shift prediction. We jointly minimize the Self-supervised shift loss L_s and occupancy loss L_o :

$$\mathcal{L}_s = \frac{1}{n} \sum_{i \in \mathcal{F}} \sum_{i=1}^n |s_i - s_i^*| \quad (11)$$

$$\mathcal{L}_o = \frac{1}{n} \sum_{i=1}^n |g_i - g_i^*| \quad (12)$$

$$\mathcal{L} = \mathcal{L}_s + \mathcal{L}_o \quad (13)$$

where s_i is the predicted shift for point $X_i \in \mathbb{R}^3$, and s_i^* is the added noise. g_i is the predicted occupancy, and g_i^* is the ground truth occupancy. Our ablation study demonstrate such training strategy contributes to higher reconstruction accuracy.

3.5 Texture Inference

After recovering the mesh of the target frame, we warp reconstructed vertices to each reference frames to fetch image feature

extracted by another image encoder. We also concatenate this feature with the geometry feature and than use MLP to predict the vertex color, which is similar to the process of occupancy prediction.

4 EXPERIMENTS

4.1 Datasets

Our goal is to reconstruct complete human model from RGB sequence, but there are few high-quality 4D public datasets. To solve it, We collect 1123 and 317 human scans from RenderPeople [43] dataset and THuman2.0 [54] dataset respectively, which contain high-quality textured human meshes, complex clothing (e.g. long skirts and down jackets) and challenging poses, then we render the scans in these two datasets using a perspective camera model, and rotate the human model for 360 degrees in yaw axis. We split our RenderPeople dataset into a training set of 1040 subjects and a testing set of 83 subjects. Our model for evaluation are trained with our Renderpeople training set. THuman2.0 dataset and RenderPeople testing set are used for evaluation.

4.2 Implementation Details

For multi-frame image feature extraction, we choose HR-Net [49] as the image encoder, which outputs a 256-channel feature map. For geometry feature extraction, inspired by [40, 41, 47], we choose the SparseConvNet [15] to process the SMPL model, divide the 3D bounding box of the SMPL into voxels and obtain a 352-channel geometry feature volume. We adopt a multi-frame transformer for feature fusion and feed the fused feature to a MLP to predict occupancy, where the number of neurons in this MLP is (608, 1024,

Table 1: Comparison of our method with other state-of-the-art works.

| Methods | Input | Topological Change | Natural Deformation | Details in Invisible Regions | Texture | Loose Cloth |
|--------------------------------|-------------------------|--------------------|---------------------|------------------------------|---------|-------------|
| DoubleFusion[55] | Monocular Depth | × | × | √ | None | × |
| TexMesh[5] | Monocular RGBD | × | × | √ | √ | × |
| PIFu/PIFuHD[44, 45] | Monocular RGB | √ | √ | × | √ | √ |
| Multi-view PIFu/PIFuHD[44, 45] | Multiple Calibrated RGB | √ | √ | √ | √ | √ |
| PaMIR[60] | Monocular RGB | √ | √ | × | √ | √ |
| Multi-frame PaMIR[60] | Monocular RGB | √ | √ | √(limited) | √ | × |
| POSEFusion[28] | Monocular RGBD | √ | √ | √ | √ | √(limited) |
| OURS | Monocular RGB | √ | √ | √ | √ | √ |

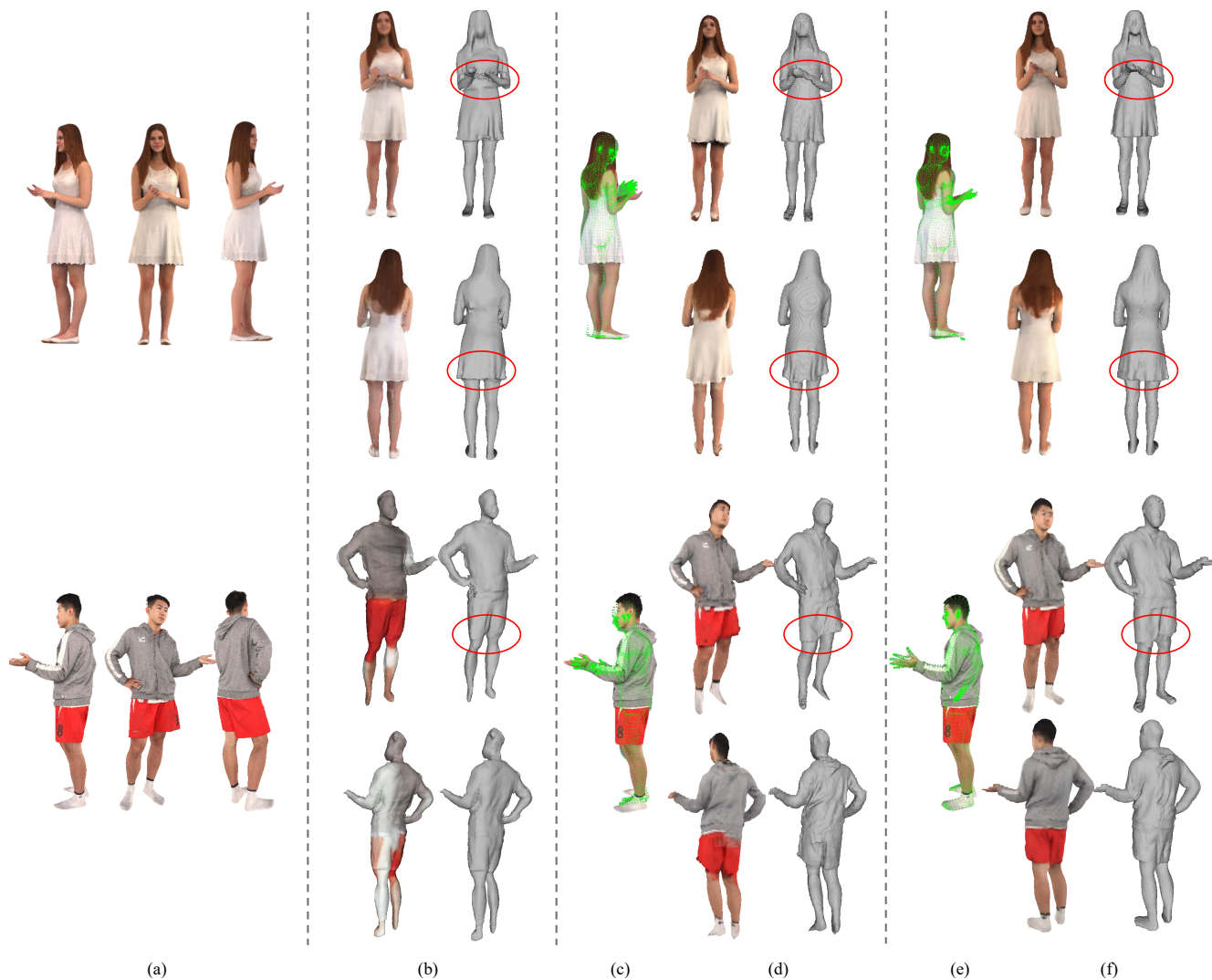


Figure 6: Qualitative comparison with SOTA methods (a) three images of the input sequence (b) Multi-Frame PaMIR (c) estimated SMPL vertices projected on image (d) ours with estimated SMPL (e) GT SMPL vertices projected on image (f) ours with GT SMPL.

Table 2: Quantitative results on RenderPeople and THuman2.0 dataset.

| | Renderpeople | | THuman2.0 | |
|------------------------|--------------|------|-----------|------|
| | Chamfer↓ | P2S↓ | Chamfer↓ | P2S↓ |
| Octopus[2] | 5.77 | 5.63 | 5.84 | 6.02 |
| Multi-view PIFu[44]* | 0.77 | 0.79 | 1.88 | 2.16 |
| Multi-frame PaMIR[60] | 1.90 | 2.33 | 5.37 | 5.11 |
| Ours w/ estimated SMPL | 0.75 | 0.81 | 2.14 | 2.32 |
| Ours w/ GT SMPL† | 0.63 | 0.76 | 1.80 | 2.02 |

* Multi-view PIFu requires well-calibrated multi-view input, other methods only require monocular RGB sequence. † Our results with GT SMPL indicates the upper bound of our method.

512, 256, 128, 1). For the texture network, we extract multi-frame image feature and stack it with previous geometry feature volume. The decoder is implemented as a MLP, where the number of neurons is (864, 1024, 512, 256, 128, 3). The number of neurons in the MLP for noise shift prediction is (256, 512, 256, 128, 3). The artificially added noise shift is generated by Gaussian distribution.

To evaluate our CrossHuman, we use multi-frame images as input, which are rendered using a perspective camera model or a weak-perspective camera model, and we selected images of challenging poses or complex clothing as input to demonstrate the robustness of our network. What is more, we use real world data to demonstrate the generalization ability of our network.

5 EVALUATIONS

5.1 Results on Real Video

We demonstrate our method for dynamic high-quality 3D human reconstruction in Fig. 5. The input is a real RGB video, and human poses are continuously changed in frames. The results demonstrate our CrossHuman trained with static synthetic data without nonrigid pose change among frames can generalize well on real video data and achieve high quality dynamic results. The video results can be seen in the supplementary material.

5.2 Comparisons

As is shown in Table. 1, our method inherits all the advantages of other SOTA human reconstruction methods while avoiding their drawbacks. Moreover, our method can be reproduced with inexpensive hardware and convenient settings. In Fig. 6, We qualitatively compare our approach with Multi-frame PaMIR [60] which is a state-of-the-art method to recover 3D human from multi frame images. Besides, We present the results of our method under estimated SMPL and ground truth SMPL (We register SMPL to scans to obtain ground truth SMPL). It is obvious that wide topological changes like the fluttering gym shorts give PaMIR a lot of trouble, while CrossHuman with MFT and warp refinement is able to handle natural deformation and topological change. The results prove our CrossHuman can recover high-fidelity details under challenging poses and loose clothes. Meanwhile, our method can ensure good performance even under imperfect SMPL. The visualization on column (c) shows the estimated SMPL vertices cannot align well with the target human on image plane, including hands region, feet region and face. CrossHuman can still generate plausible and detailed

Table 3: Quantitative evaluations on Renderpeople dataset with estimated SMPL.

| | Chamfer↓ | P2S↓ |
|--------------------------------|----------|------|
| average pooling | 1.11 | 1.73 |
| self-attention | 0.96 | 1.02 |
| ours (MFT wo/ warp refinement) | 0.83 | 0.90 |
| ours (MFT w/ warp refinement) | 0.75 | 0.81 |

results. Such SMPL fault tolerance makes our method applicable in a wider range of conditions. In addition, we conduct quantitative comparison in Table. 2. We compute point-to-surface Euclidean distance (P2S) in cm from the vertices on the reconstructed mesh to the ground truth. We also compute Chamfer distance in cm from the reconstructed mesh and the ground truth mesh. Results in the Table. 2 demonstrate our method improves the reconstruction accuracy. The multi-view PIFu listed in Table. 2 requires well calibrated cameras.

5.3 Ablation study

To figure out the strength of our multi-frame transformer, we train another two models with average pooling feature fusion used in PIFu[44] and self-attention based feature fusion strategy used in PixelNerf [52] and DeepMultiCap [59]. The results in Fig. 7 demonstrate that our method with MFT can effectively recover more surface detail in both visible and invisible regions. In addition, we conduct comparative experiments to verify the effect of the self-supervised warp refinement training module. Fig. 8 illustrates the results of our method on real video data with and without warp refinement module under inaccurate SMPL estimation, which prove the warp refinement training module can effectively reduce some artifacts and blurring caused by tracking errors. Owing to these two modules, CrossHuman is able to generate visually coherent and robust reconstruction results in most cases including cases with loose cloth and challenging poses. Results in Table. 3 gives quantitative evidence of the effectiveness of our MFT and warp refinement scheme. We also conduct an ablation experiment on the THuman dataset for tuning the appropriate number of reference frames. As is shown in Fig. 9, the larger number of reference frames doesn't necessarily lead to better performance, since the multi-frame feature fusion will produce a smoothing effect.

5.4 Limitation and Discussion

Many previous monocular human reconstruction methods combined with implicit function and parametric models did not obtain satisfactory robustness especially for challenging poses. A key difficulty is to ensure the perfect alignment between the parametric body and the human on the image, which is not easy on 2D image plane and even harder in 3D space due to depth ambiguity. From the point of view of the practicality of the algorithm, we sidestep this problem by regularizing the reconstructed geometry with parametric body strictly. To be more specific, our CrossHuman always trust the input parametric body no matter whether it is accurate or not and rely on MFT and warp refinement to deal with tracking error. As a result, we can always get plausible results without mutilated limb even under the rough alignment. This strategy is

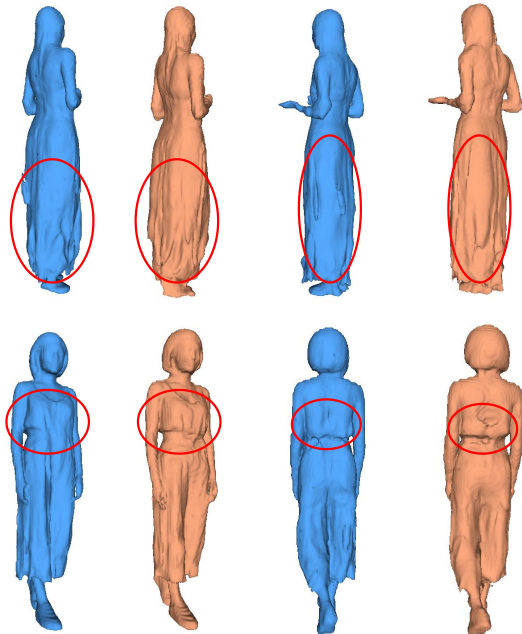


Figure 7: Qualitative evaluation on feature fusion module. The blue models are our reconstructions with self-attention block, and the orange models are our reconstructions with MFT.



Figure 8: Qualitative evaluation of warp refinement module on real video (a) two frames of input sequence (b) our reconstruction results wo/ warp refinement (c) our reconstruction results w/ warp refinement.

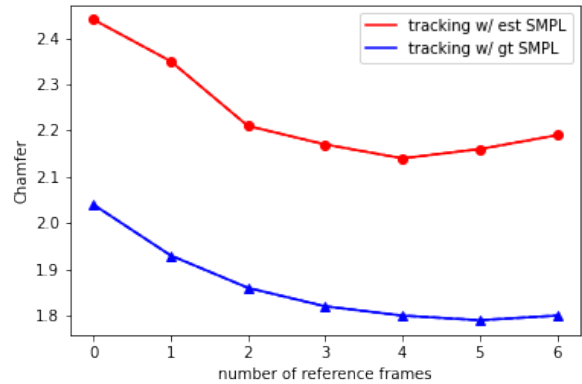


Figure 9: Evaluation of the number of reference frames

visually successful but still a stopgap, making the quantitative reconstruction accuracy subject to the SMPL accuracy. A possible more comprehensive solution could be an end-to-end method to jointly infer the parametric body and detailed surface with mandatory alignment. Besides, though our CrossHuman trained on static data generalize well on real-video with non-rigid deformation, the details of invisible regions are not natural enough in some cases. A model trained with 4D dataset is expected to handle more natural non-rigid deformation.

6 CONCLUSION

In this paper, we propose CrossHuman, the method that learns cross-guidance from RGB sequence and corresponding parametric human model to achieve high-quality human 3D reconstruction from a single RGB camera. we propose a new self-supervised warp refinement scheme and a novel multi-frame transformer to relax the requirement of SMPL model accuracy, leading to the robust performance in case of very loose cloth even under imperfect SMPL estimation. The detailed dynamic reconstruction results on real video prove the good generalization of our method. We believe our work will contribute to the development of cost-effective 3D human reconstruction, providing more possibilities for consumer-grade VR/AR applications and immersive entertainment or communication.

REFERENCES

- [1] Kara-Ali Aliev, Artem Sevastopolsky, Maria Kolos, Dmitry Ulyanov, and Victor Lempitsky. 2020. Neural point-based graphics. In *Computer Vision–ECCV 2020: 16th European Conference, Glasgow, UK, August 23–28, 2020, Proceedings, Part XXII* 16. Springer, 696–712.
- [2] Thiemo Alldieck, Marcus Magnor, Bharat Lal Bhatnagar, Christian Theobalt, and Gerard Pons-Moll. 2019. Learning to reconstruct people in clothing from a single RGB camera. In *Proceedings of the IEEE/CVF Conference on Computer Vision and Pattern Recognition*. 1175–1186.
- [3] Thiemo Alldieck, Marcus Magnor, Weipeng Xu, Christian Theobalt, and Gerard Pons-Moll. 2018. Detailed human avatars from monocular video. In *2018 International Conference on 3D Vision (3DV)*. IEEE, 98–109.
- [4] Thiemo Alldieck, Marcus Magnor, Weipeng Xu, Christian Theobalt, and Gerard Pons-Moll. 2018. Video based reconstruction of 3d people models. In *Proceedings of the IEEE Conference on Computer Vision and Pattern Recognition*. 8387–8397.
- [5] Thiemo Alldieck, Gerard Pons-Moll, Christian Theobalt, and Marcus Magnor. 2019. Tex2shape: Detailed full human body geometry from a single image. In *Proceedings of the IEEE/CVF International Conference on Computer Vision*. 2293–2303.
- [6] Bharat Lal Bhatnagar, Cristian Sminchisescu, Christian Theobalt, and Gerard Pons-Moll. 2020. Combining implicit function learning and parametric models for 3d human reconstruction. In *Computer Vision–ECCV 2020: 16th European Conference, Glasgow, UK, August 23–28, 2020, Proceedings, Part II* 16. Springer, 311–329.
- [7] Federica Bogo, Angjoo Kanazawa, Christoph Lassner, Peter Gehler, Javier Romero, and Michael J Black. 2016. Keep it SMPL: Automatic estimation of 3D human pose and shape from a single image. In *European conference on computer vision*. Springer, 561–578.
- [8] Z. Cao, G. Hidalgo Martinez, T. Simon, S. Wei, and Y. A. Sheikh. 2019. OpenPose: Realtime Multi-Person 2D Pose Estimation using Part Affinity Fields. *IEEE Transactions on Pattern Analysis and Machine Intelligence* (2019).
- [9] Zhiqin Chen and Hao Zhang. 2019. Learning implicit fields for generative shape modeling. In *Proceedings of the IEEE/CVF Conference on Computer Vision and Pattern Recognition*. 5939–5948.
- [10] Julian Chibane, Thiemo Alldieck, and Gerard Pons-Moll. 2020. Implicit functions in feature space for 3d shape reconstruction and completion. In *Proceedings of the IEEE/CVF Conference on Computer Vision and Pattern Recognition*. 6970–6981.
- [11] Haoqiang Fan, Hao Su, and Leonidas J Guibas. 2017. A point set generation network for 3d object reconstruction from a single image. In *Proceedings of the IEEE conference on computer vision and pattern recognition*. 605–613.
- [12] Juergen Gall, Carsten Stoll, Edison De Aguiar, Christian Theobalt, Bodo Rosenhahn, and Hans-Peter Seidel. 2009. Motion capture using joint skeleton tracking and surface estimation. In *2009 IEEE Conference on Computer Vision and Pattern Recognition*. IEEE, 1746–1753.
- [13] Kyle Genova, Forrester Cole, Avneesh Sud, Aaron Sarna, and Thomas Funkhouser. 2020. Local deep implicit functions for 3d shape. In *Proceedings of the IEEE/CVF Conference on Computer Vision and Pattern Recognition*. 4857–4866.
- [14] Rohit Girdhar, David F Fouhey, Mikel Rodriguez, and Abhinav Gupta. 2016. Learning a predictable and generative vector representation for objects. In *European Conference on Computer Vision*. Springer, 484–499.
- [15] Benjamin Graham, Martin Engelcke, and Laurens Van Der Maaten. 2018. 3d semantic segmentation with submanifold sparse convolutional networks. In *Proceedings of the IEEE conference on computer vision and pattern recognition*. 9224–9232.
- [16] Kaiwen Guo, Peter Lincoln, Philip Davidson, Jay Busch, Xueming Yu, Matt Whalen, Geoff Harvey, Sergio Orts-Escolano, Rohit Pandey, Jason Dourgarian, et al. 2019. The reightables: Volumetric performance capture of humans with realistic relighting. *ACM Transactions on Graphics (TOG)* 38, 6 (2019), 1–19.
- [17] Marc Habermann, Weipeng Xu, Michael Zollhofer, Gerard Pons-Moll, and Christian Theobalt. 2019. Livecap: Real-time human performance capture from monocular video. *ACM Transactions On Graphics (TOG)* 38, 2 (2019), 1–17.
- [18] Marc Habermann, Weipeng Xu, Michael Zollhofer, Gerard Pons-Moll, and Christian Theobalt. 2020. Deepcap: Monocular human performance capture using weak supervision. In *Proceedings of the IEEE/CVF Conference on Computer Vision and Pattern Recognition*. 5052–5063.
- [19] Tong He, John Collomosse, Hailin Jin, and Stefano Soatto. 2020. Geo-pifu: Geometry and pixel aligned implicit functions for single-view human reconstruction. *arXiv preprint arXiv:2006.08072* (2020).
- [20] Tong He, Yuanlu Xu, Shunsuke Saito, Stefano Soatto, and Tony Tung. 2021. ARCH++: Animation-ready clothed human reconstruction revisited. In *Proceedings of the IEEE/CVF International Conference on Computer Vision*. 11046–11056.
- [21] Zeng Huang, Yuanlu Xu, Christoph Lassner, Hao Li, and Tony Tung. 2020. Arch: Animatable reconstruction of clothed humans. In *Proceedings of the IEEE/CVF Conference on Computer Vision and Pattern Recognition*. 3093–3102.
- [22] Chiyu Jiang, Avneesh Sud, Ameesh Makadia, Jingwei Huang, Matthias Nießner, Thomas Funkhouser, et al. 2020. Local implicit grid representations for 3d scenes. In *Proceedings of the IEEE/CVF Conference on Computer Vision and Pattern Recognition*. 6001–6010.
- [23] Angjoo Kanazawa, Michael J Black, David W Jacobs, and Jitendra Malik. 2018. End-to-end recovery of human shape and pose. In *Proceedings of the IEEE conference on computer vision and pattern recognition*. 7122–7131.
- [24] Muhammed Kocabas, Nikos Athanasiou, and Michael J Black. 2020. Vibe: Video inference for human body pose and shape estimation. In *Proceedings of the IEEE/CVF Conference on Computer Vision and Pattern Recognition*. 5253–5263.
- [25] Nikos Kolotouros, Georgios Pavlakos, Michael J Black, and Kostas Daniilidis. 2019. Learning to reconstruct 3D human pose and shape via model-fitting in the loop. In *Proceedings of the IEEE/CVF International Conference on Computer Vision*. 2252–2261.
- [26] Verica Lazova, Eldar Insafutdinov, and Gerard Pons-Moll. 2019. 360-degree textures of people in clothing from a single image. In *2019 International Conference on 3D Vision (3DV)*. IEEE, 643–653.
- [27] Vincent Leroy, Jean-Sébastien Franco, and Edmond Boyer. 2017. Multi-view dynamic shape refinement using local temporal integration. In *Proceedings of the IEEE international conference on computer vision*. 3094–3103.
- [28] Zhe Li, Tao Yu, Zerong Zheng, Kaiwen Guo, and Yebin Liu. 2021. POSEfusion: Pose-guided Selective Fusion for Single-view Human Volumetric Capture. In *Proceedings of the IEEE/CVF Conference on Computer Vision and Pattern Recognition*. 14162–14172.
- [29] Chen-Hsuan Lin, Chen Kong, and Simon Lucey. 2018. Learning efficient point cloud generation for dense 3d object reconstruction. In *proceedings of the AAAI Conference on Artificial Intelligence*, Vol. 32.
- [30] Shanchuan Lin, Andrey Ryabtsev, Soumyadip Sengupta, Brian Curless, Steve Seitz, and Ira Kemelmacher-Shlizerman. 2020. Real-Time High-Resolution Background Matting. *arXiv* (2020), arXiv–2012.
- [31] Yebin Liu, Juergen Gall, Carsten Stoll, Qionghai Dai, Hans-Peter Seidel, and Christian Theobalt. 2013. Markerless motion capture of multiple characters using multiview image segmentation. *IEEE transactions on pattern analysis and machine intelligence* 35, 11 (2013), 2720–2735.
- [32] Stephen Lombardi, Tomas Simon, Jason Saragih, Gabriel Schwartz, Andreas Lehrmann, and Yaser Sheikh. 2019. Neural volumes: Learning dynamic renderable volumes from images. *arXiv preprint arXiv:1906.07751* (2019).
- [33] Matthew Loper, Naureen Mahmood, Javier Romero, Gerard Pons-Moll, and Michael J Black. 2015. SMPL: A skinned multi-person linear model. *ACM transactions on graphics (TOG)* 34, 6 (2015), 1–16.
- [34] William E Lorensen and Harvey E Cline. 1987. Marching cubes: A high resolution 3D surface construction algorithm. *ACM siggraph computer graphics* 21, 4 (1987), 163–169.
- [35] Qianli Ma, Jinlong Yang, Anurag Ranjan, Sergi Pujades, Gerard Pons-Moll, Siyu Tang, and Michael J Black. 2020. Learning to dress 3d people in generative clothing. In *Proceedings of the IEEE/CVF Conference on Computer Vision and Pattern Recognition*. 6469–6478.
- [36] Armin Mustafa, Hansung Kim, Jean-Yves Guillemaut, and Adrian Hilton. 2015. General dynamic scene reconstruction from multiple view video. In *Proceedings of the IEEE International Conference on Computer Vision*. 900–908.
- [37] Richard A Newcombe, Dieter Fox, and Steven M Seitz. 2015. Dynamicfusion: Reconstruction and tracking of non-rigid scenes in real-time. In *Proceedings of the IEEE conference on computer vision and pattern recognition*. 343–352.
- [38] Ahmed AA Osman, Timo Bolkart, and Michael J Black. 2020. Star: Sparse trained articulated human body regressor. In *Computer Vision–ECCV 2020: 16th European Conference, Glasgow, UK, August 23–28, 2020, Proceedings, Part VI* 16. Springer, 598–613.
- [39] Jeong Joon Park, Peter Florence, Julian Straub, Richard Newcombe, and Steven Lovegrove. 2019. DeepSDF: Learning continuous signed distance functions for shape representation. In *Proceedings of the IEEE/CVF Conference on Computer Vision and Pattern Recognition*. 165–174.
- [40] Songyou Peng, Michael Niemeyer, Lars Mescheder, Marc Pollefeys, and Andreas Geiger. 2020. Convolutional occupancy networks. In *Computer Vision–ECCV 2020: 16th European Conference, Glasgow, UK, August 23–28, 2020, Proceedings, Part III* 16. Springer, 523–540.
- [41] Sida Peng, Yuanqing Zhang, Yinghao Xu, Qianqian Wang, Qing Shuai, Hujun Bao, and Xiaowei Zhou. 2021. Neural body: Implicit neural representations with structured latent codes for novel view synthesis of dynamic humans. In *Proceedings of the IEEE/CVF Conference on Computer Vision and Pattern Recognition*. 9054–9063.
- [42] Charles R Qi, Hao Su, Kaichun Mo, and Leonidas J Guibas. 2017. Pointnet: Deep learning on point sets for 3d classification and segmentation. In *Proceedings of the IEEE conference on computer vision and pattern recognition*. 652–660.
- [43] renderpeople. 2000. <https://renderpeople.com/>.
- [44] Shunsuke Saito, Zeng Huang, Ryota Natsume, Shigeo Morishima, Angjoo Kanazawa, and Hao Li. 2019. Pifu: Pixel-aligned implicit function for high-resolution clothed human digitization. In *Proceedings of the IEEE/CVF International Conference on Computer Vision*. 2304–2314.

- [45] Shunsuke Saito, Tomas Simon, Jason Saragih, and Hanbyul Joo. 2020. Pifuhd: Multi-level pixel-aligned implicit function for high-resolution 3d human digitization. In *Proceedings of the IEEE/CVF Conference on Computer Vision and Pattern Recognition*. 84–93.
- [46] Ruizhi Shao, Hongwen Zhang, He Zhang, Yanpei Cao, Tao Yu, and Yebin Liu. 2021. DoubleField: Bridging the Neural Surface and Radiance Fields for High-fidelity Human Rendering. *arXiv preprint arXiv:2106.03798* (2021).
- [47] Shaoshuai Shi, Chaoxu Guo, Li Jiang, Zhe Wang, Jianping Shi, Xiaogang Wang, and Hongsheng Li. 2020. Pv-rcnn: Point-voxel feature set abstraction for 3d object detection. In *Proceedings of the IEEE/CVF Conference on Computer Vision and Pattern Recognition*. 10529–10538.
- [48] Vincent Sitzmann, Justus Thies, Felix Heide, Matthias Nießner, Gordon Wetzstein, and Michael Zollhofer. 2019. Deepvoxels: Learning persistent 3d feature embeddings. In *Proceedings of the IEEE/CVF Conference on Computer Vision and Pattern Recognition*. 2437–2446.
- [49] Ke Sun, Bin Xiao, Dong Liu, and Jingdong Wang. 2019. Deep high-resolution representation learning for human pose estimation. In *Proceedings of the IEEE/CVF Conference on Computer Vision and Pattern Recognition*. 5693–5703.
- [50] Lan Xu, Wei Cheng, Kaiwen Guo, Lei Han, Yebin Liu, and Lu Fang. 2019. Flyfusion: Realtime dynamic scene reconstruction using a flying depth camera. *IEEE transactions on visualization and computer graphics* 27, 1 (2019), 68–82.
- [51] Kinchen Yan, Jimei Yang, Ersin Yumer, Yijie Guo, and Honglak Lee. 2016. Perspective transformer nets: Learning single-view 3d object reconstruction without 3d supervision. *arXiv preprint arXiv:1612.00814* (2016).
- [52] Alex Yu, Vickie Ye, Matthew Tancik, and Angjoo Kanazawa. 2021. pixelnerf: Neural radiance fields from one or few images. In *Proceedings of the IEEE/CVF Conference on Computer Vision and Pattern Recognition*. 4578–4587.
- [53] Tao Yu, Kaiwen Guo, Feng Xu, Yuan Dong, Zhaoqi Su, Jianhui Zhao, Jianguo Li, Qionghai Dai, and Yebin Liu. 2017. Bodyfusion: Real-time capture of human motion and surface geometry using a single depth camera. In *Proceedings of the IEEE International Conference on Computer Vision*. 910–919.
- [54] Tao Yu, Zerong Zheng, Kaiwen Guo, Pengpeng Liu, Qionghai Dai, and Yebin Liu. 2021. Function4D: Real-time Human Volumetric Capture from Very Sparse Consumer RGBD Sensors. In *Proceedings of the IEEE/CVF Conference on Computer Vision and Pattern Recognition*. 5746–5756.
- [55] Tao Yu, Zerong Zheng, Kaiwen Guo, Jianhui Zhao, Qionghai Dai, Hao Li, Gerard Pons-Moll, and Yebin Liu. 2018. Doublefusion: Real-time capture of human performances with inner body shapes from a single depth sensor. In *Proceedings of the IEEE conference on computer vision and pattern recognition*. 7287–7296.
- [56] Wang Zeng, Wanli Ouyang, Ping Luo, Wentao Liu, and Xiaogang Wang. 2020. 3d human mesh regression with dense correspondence. In *Proceedings of the IEEE/CVF Conference on Computer Vision and Pattern Recognition*. 7054–7063.
- [57] Chao Zhang, Sergi Pujades, Michael J Black, and Gerard Pons-Moll. 2017. Detailed, accurate, human shape estimation from clothed 3D scan sequences. In *Proceedings of the IEEE Conference on Computer Vision and Pattern Recognition*. 4191–4200.
- [58] Hongwen Zhang, Yating Tian, Xinchu Zhou, Wanli Ouyang, Yebin Liu, Limin Wang, and Zhenan Sun. 2021. Pymaf: 3d human pose and shape regression with pyramidal mesh alignment feedback loop. In *Proceedings of the IEEE/CVF International Conference on Computer Vision*. 11446–11456.
- [59] Yang Zheng, Ruizhi Shao, Yuxiang Zhang, Tao Yu, Zerong Zheng, Qionghai Dai, and Yebin Liu. 2021. DeepMultiCap: Performance Capture of Multiple Characters Using Sparse Multiview Cameras. *arXiv preprint arXiv:2105.00261* (2021).
- [60] Zerong Zheng, Tao Yu, Yebin Liu, and Qionghai Dai. 2021. Pamir: Parametric model-conditioned implicit representation for image-based human reconstruction. *IEEE Transactions on Pattern Analysis and Machine Intelligence* (2021).
- [61] Tiancheng Zhi, Christoph Lassner, Tony Tung, Carsten Stoll, Srinivasa G Narasimhan, and Minh Vo. 2020. Texmesh: Reconstructing detailed human texture and geometry from rgb-d video. In *European Conference on Computer Vision*. Springer, 492–509.

A APPENDIX

A.1 Generation of Ground Truth SMPL

In our experiments, we register SMPL models to 3D scans in our dataset to obtain accurate SPML parameters and corresponding 3D models. The registered SMPL models are described as ground truth SMPL in our paper. To achieve reliable registrations, we optimize SMPL parameters iteratively by minimizing the chamfer loss between SMPL vertices and scan vertices together with 2D joints loss between semantic-aligned SMPL body joints projected on images and 2D keypoints extracted by Openpose [8].

A.2 Additional Results

Additional Qualitative Results We present additional qualitative results in Fig.10 to further demonstrate the effectiveness of our CrossHuman.

Video Results We provide supplemental videos of dynamic reconstruction from self-captured videos. Results on some of the frames are presented in Fig. 11. The backgrounds of videos are removed by BackgroundMattingV2 [30].

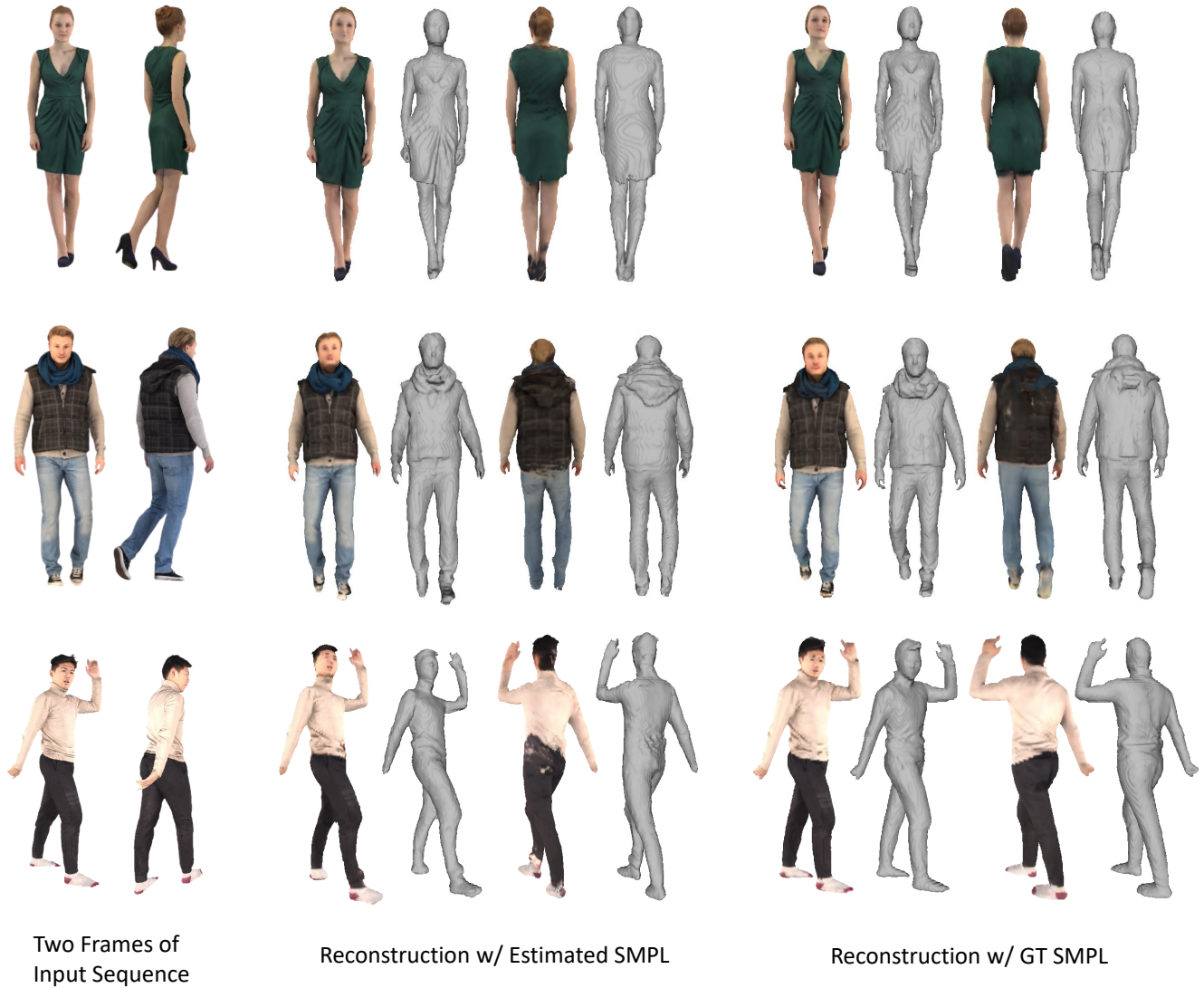
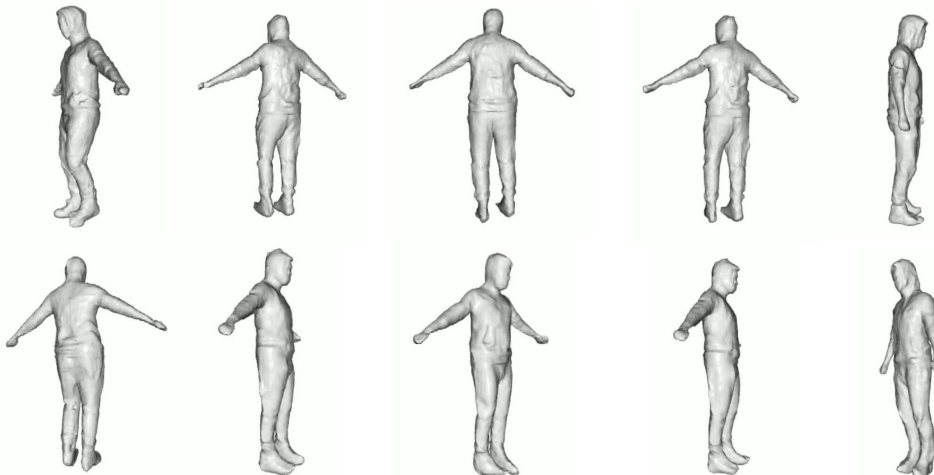


Figure 10: More results on synthetic data

Input Frames



Reconstructions



Input Frames



Reconstructions

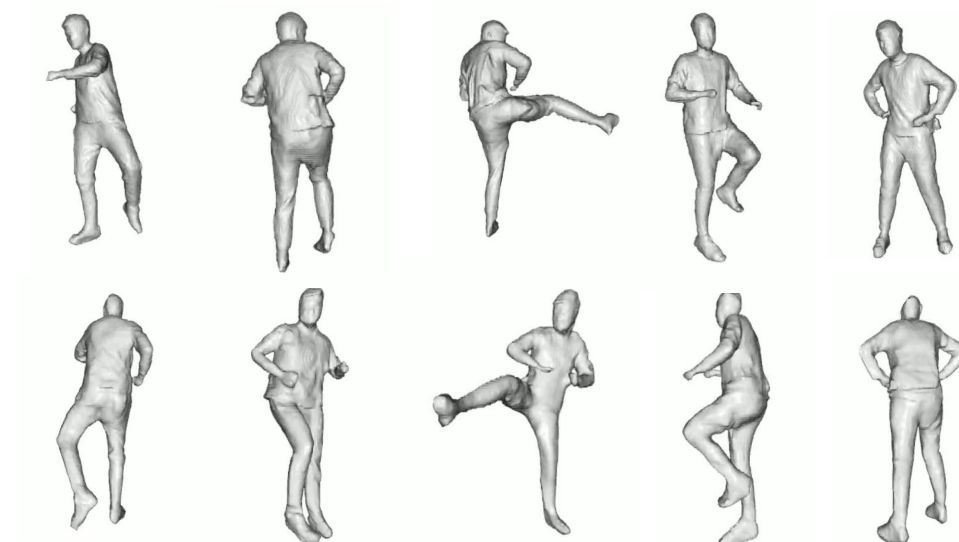


Figure 11: Results on Real Video